

Real-time dynamics of Auger wavepackets and decays in ultrafast charge migration processes

F. Covito,¹ E. Perfetto,^{2,3} A. Rubio,^{1,4,5} and G. Stefanucci^{3,6}

¹*Max Planck Institute for the Structure and Dynamics of Matter and Center for Free-Electron Laser Science, Luruper Chaussee 149, 22761 Hamburg, Germany*

²*CNR-ISM, Division of Ultrafast Processes in Materials (FLASHit), Area della ricerca di Roma 1, Monterotondo Scalo, Italy*

³*Dipartimento di Fisica, Università di Roma Tor Vergata, Via della Ricerca Scientifica, 00133 Rome, Italy*

⁴*Center for Computational Quantum Physics (CCQ), The Flatiron Institute, 162 Fifth avenue, New York NY 10010*

⁵*Nano-Bio Spectroscopy Group, Universidad del País Vasco, 20018 San Sebastian, Spain*

⁶*INFN, Sezione di Roma Tor Vergata, Via della Ricerca Scientifica 1, 00133 Roma, Italy*
(Dated: February 27, 2022)

The Auger decay is a relevant recombination channel during the first few femtoseconds of molecular targets impinged by attosecond XUV or soft X-ray pulses. Including this mechanism in time-dependent simulations of charge-migration processes is a difficult task, and Auger scatterings are often ignored altogether. In this work we present an advance of the current state-of-the-art by putting forward a real-time approach based on nonequilibrium Green's functions suitable for first-principles calculations of molecules with tens of active electrons. To demonstrate the accuracy of the method we report comparisons against accurate grid simulations of one-dimensional systems. We also predict a highly asymmetric profile of the Auger wavepacket, with a long tail exhibiting ripples temporally spaced by the inverse of the Auger energy.

The sub-femtosecond dynamics of the hole density created by an ionizing attosecond XUV or soft X-ray pulse precedes any nuclear rearrangement and dictates the relaxation pathways of the underlying molecular structure [1, 2]. This ultrafast charge oscillation, also referred to as ultrafast charge migration (UCM), is driven exclusively by electronic correlations up to a few femtoseconds [3–7]. At these time scales the Auger scattering is the only possible energy-dissipation mechanism and, in addition to shake-up and polarization effects [8], a relevant recombination channel.

Recent advances in pump-probe spectroscopy made possible to follow the Auger decay in atomic targets [2, 9–12]. Accurate measurements have been performed and successfully interpreted in terms of transitions between excited cationic states. The theory behind these experiments shows that the Auger electron is a “courier” of the complex dynamics occurring in the parent cation [13–15]. Unfortunately, *ab initio* analysis relying on many-electron eigenfunctions and eigenvalues are possible for single atoms but become soon prohibitive for larger systems. In fact, first-principles approaches that include Auger scatterings in the UCM dynamics of molecules have not yet been developed.

Time-Dependent Density Functional Theory [16–18] (TDDFT) is the method of choice for large scale simulations. However, the vast majority of TDDFT calculations are performed using an adiabatic exchange-correlation (xc) potential, i.e., a functional of the instantaneous density. As shown in Ref. [19], adiabatic approximations are unable to capture the Auger effect [20]. Learning how to include memory effects in the xc functional is a major line of research to which the present work could provide

new insights.

In this Letter we lay down a first-principles real-time NonEquilibrium Green's Function [21, 22] (NEGF) approach which incorporates Auger scatterings in the UCM dynamics of molecules hit by attosecond pulses. In analogy with the NEGF formulation of quantum transport where the dynamics of electrons in the junction is simulated without dealing explicitly with the electrons in the leads [23–25], we close the NEGF equations on the molecule and deal only partially with the degrees of freedom of the Auger electrons. The computational effort changes slightly with respect to previous NEGF implementations [26–28], thereby making possible to simulate the UCM of molecules with tens of active electrons.

We demonstrate that the approach well captures qualitative and quantitative aspects of the Auger physics through comparisons against real-time simulations of one-dimensional (1D) atoms on a grid. The Auger wavepacket can, in principle, be reconstructed from NEGF through a postprocessing procedure. For 3D molecules such procedure is numerically (too) demanding but for the considered 1D atom the calculation is doable and the agreement with the full-grid results is again satisfactory. Interestingly, we highlight a universal feature of the asymmetric Auger wavepacket, namely a long tail with superimposed ripples temporally spaced by the inverse of the Auger energy.

Method: We consider a finite system (an atom or molecule) with single-particle Hartree-Fock (HF) basis $\varphi_i(\mathbf{r})$ for bound electrons and $\varphi_\mu(\mathbf{r})$ for electrons in the continuum (for simplicity we work with spin-degenerate systems). Let $\hat{c}_{i\sigma}$ ($\hat{c}_{\mu\sigma}$) be the annihilation operator for an electron on φ_i (φ_μ) with spin σ . In the absence of

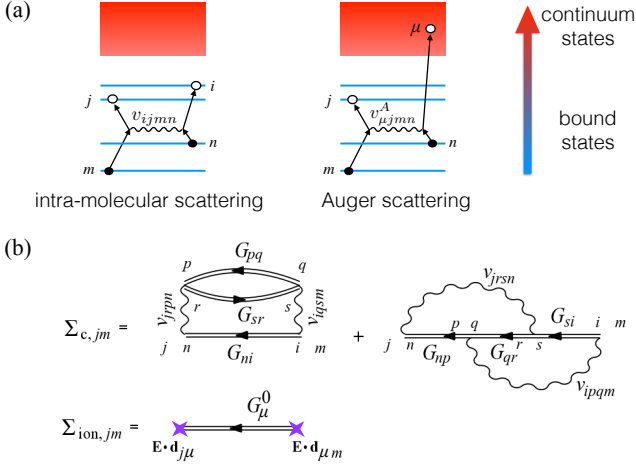


FIG. 1: (a) Schematic illustration of intra-molecular (left) and Auger (right) scattering. (b) Correlation self-energy in the 2B approximation (top) and ionization self-energy (bottom).

external fields the total Hamiltonian

$$\hat{H}^{\text{eq}} = \hat{H}_{\text{bound}} + \hat{H}_{\text{Auger}} + \hat{H}_{\text{cont}} \quad (1)$$

is the sum of the bound-electrons Hamiltonian $\hat{H}_{\text{bound}} = \sum_{ij} h_{ij} \hat{c}_{i\sigma}^\dagger \hat{c}_{j\sigma} + \frac{1}{2} \sum_{ijmn} v_{ijmn} \hat{c}_{i\sigma}^\dagger \hat{c}_{j\sigma'}^\dagger \hat{c}_{m\sigma'} \hat{c}_{n\sigma}$, the Auger interaction $\hat{H}_{\text{Auger}} = \sum_{ijm\mu} v_{ijm\mu}^A \left(\hat{c}_{i\sigma}^\dagger \hat{c}_{j\sigma'}^\dagger \hat{c}_{m\sigma'} \hat{c}_{\mu\sigma} + \text{h.c.} \right)$ and a free-continuum part $\hat{H}_{\text{cont}} = \sum_{\mu\sigma} \epsilon_\mu \hat{c}_{\mu\sigma}^\dagger \hat{c}_{\mu\sigma}$. Here h_{ij} are the one-electron integrals, ϵ_μ are the continuum single-particle energies and v_{ijmn} ($v_{ijm\mu}^A$) are the four-index Coulomb integrals responsible for intra-molecular (Auger) scatterings, see Fig. 1(a).

The system is perturbed either by the sudden removal of a bound electron or by an external laser field. In the dipole approximation the laser-system interaction reads

$$\hat{H}^{\text{E}}(t) = \hat{H}_{\text{bound}}^{\text{E}}(t) + \hat{H}_{\text{ion}}^{\text{E}}(t), \quad (2)$$

where $\hat{H}_{\text{bound}}^{\text{E}}(t) = \mathbf{E}(t) \cdot \sum_{ij} \mathbf{d}_{ij} \hat{c}_{i\sigma}^\dagger \hat{c}_{j\sigma}$ describes intra-molecular transitions whereas $\hat{H}_{\text{ion}}^{\text{E}}(t) = \mathbf{E}(t) \cdot \sum_{i\mu} \left(\mathbf{d}_{i\mu} \hat{c}_{i\sigma}^\dagger \hat{c}_{\mu\sigma} + \text{h.c.} \right)$ is responsible for ionization. The vector \mathbf{d}_{ij} ($\mathbf{d}_{i\mu}$) is the matrix element of the dipole operator between states φ_i and φ_j (φ_μ). In Eqs. (1) and (2) we are discarding the off-diagonal elements $h_{i\mu}$, $h_{\mu\mu'}$ and $\mathbf{d}_{\mu\mu'}$ as well as all Coulomb integrals with two or more indices in the continuum. We anticipate that this simplification affects only marginally the results presented below.

The electron dynamics is simulated using NEGF. Without Auger scatterings the equation of motion for the one-particle density matrix $\rho_{ij}(t) = \langle \hat{c}_{j\sigma}^\dagger(t) \hat{c}_{i\sigma}(t) \rangle$ (with indices in the bound sector) has been derived elsewhere [26] and reads $\dot{\rho} = -i[h_{\text{HF}}[\rho], \rho] - \mathcal{I}[\rho] - \mathcal{I}^\dagger[\rho]$.

Here the HF Hamiltonian $h_{\text{HF}}(t) \equiv h + V_{\text{HF}}(t) + \mathbf{E}(t) \cdot \mathbf{d}$ is a functional of ρ through the HF potential $V_{\text{HF},ij}(t) = \sum_{mn} \rho_{nm}(t) w_{imnj}$, with $w_{imnj} \equiv 2v_{imnj} - v_{imjn}$. Dynamical correlation and ionization processes are described by the generalized collision integral

$$\mathcal{I}(t) = \int_0^t d\bar{t} [\Sigma^>(t, \bar{t}) G^<(\bar{t}, t) - \Sigma^<(t, \bar{t}) G^>(\bar{t}, t)], \quad (3)$$

where $\Sigma^{\lessgtr} \equiv \Sigma_c^{\lessgtr} + \Sigma_{\text{ion}}^{\lessgtr}$ is the sum of the lesser/greater correlation (Σ_c) and ionization (Σ_{ion}) self-energies. Both are time-nonlocal functionals of ρ through the Generalized Kadanoff-Baym Ansatz [29] (GKBA), see Appendix A for details. Figure 1(b) illustrates the diagrammatic representation of Σ_c in the second-Born (2B) approximation and Σ_{ion} . The computational cost of these NEGF calculations scales like $N_t^2 N_{\text{bound}}^{\text{p}}$ where N_t is the number of time-steps, N_{bound} the number of HF bound states and the power $3 \leq \text{p} \leq 5$ depends on how sparse v_{ijmn} is. Real-time simulations of, e.g., organic or biologically relevant molecules can easily be carried out up to 30 ÷ 40 femtoseconds [28].

The inclusion of Auger scattering processes leads to a coupling between the density matrix $\rho(t)$ and the occupations $f_\mu(t) = \langle \hat{c}_{\mu\sigma}^\dagger(t) \hat{c}_{\mu\sigma}(t) \rangle$ of the continuum states. For these quantities we have derived, see Appendix A, the following coupled system of NEGF equations of motion

$$\begin{cases} \dot{\rho} = -i[h_{\text{HF}}[\rho], \rho] - \mathcal{I}[\rho, f] - \mathcal{I}^\dagger[\rho, f] \\ \dot{f}_\mu = -\mathcal{J}_\mu[\rho, f] - \mathcal{J}_\mu^*[\rho, f] \end{cases} \quad (4)$$

The generalized collision integral $\mathcal{I}[\rho, f]$ is defined as in Eq. (A20) but $\Sigma[\rho] \rightarrow \Sigma[\rho] + \Sigma_{\text{Auger}}[\rho, f]$. The Auger self-energy is calculated from the second-order (in v^A) diagrams, in accordance with Refs. [30, 31], and reads

$$\begin{aligned} \Sigma_{\text{Auger},ij}^{\lessgtr}(t, \bar{t}) &= \sum_{mn} \sum_{pq} \sum_{\mu} G_{mn}^{\lessgtr}(t, \bar{t}) \\ &\times \left[G_{\mu}^{\lessgtr}(t, \bar{t}) G_{pq}^{\gtrless}(\bar{t}, t) (v_{iqm\mu}^A w_{\mu npj}^A + v_{iq\mu m}^A w_{n\mu pj}^A) \right. \\ &\quad \left. + G_{pq}^{\lessgtr}(t, \bar{t}) G_{\mu}^{\gtrless}(\bar{t}, t) v_{i\mu pm}^A w_{nq\mu j}^A \right], \end{aligned} \quad (5)$$

where we neglected the off-diagonal elements of the continuum Green's function, i.e., $G_{\mu\nu}^{\lessgtr} = \delta_{\mu\nu} G_{\mu}^{\lessgtr}$. As we shall demonstrate this approximation is remarkably accurate. Through the GKBA, Σ_{Auger} is a time-nonlocal functional of ρ and f_μ . Finally, the collision integral \mathcal{J}_μ reads

$$\mathcal{J}_\mu(t) = \int_0^t d\bar{t} [K_{\mu\mu}^>(t, \bar{t}) f_\mu^<(\bar{t}) + K_{\mu\mu}^<(t, \bar{t}) f_\mu^>(\bar{t})], \quad (6)$$

where the kernel

$$\begin{aligned} K_{\mu\nu}^{\lessgtr}(t, \bar{t}) &= i \sum_{mn} \sum_{pq} \sum_{sr} v_{\mu r p m}^A w_{n q s \nu}^A \\ &\times G_{mn}^{\lessgtr}(t, \bar{t}) G_{pq}^{\lessgtr}(t, \bar{t}) G_{sr}^{\gtrless}(\bar{t}, t) e^{-i\epsilon_\nu(\bar{t}-t)} \end{aligned} \quad (7)$$

is a time-nonlocal functional of ρ only. Equations (4), together with the definitions that follow it, constitute the first (methodological) result of this Letter. The implementation of Eqs. (4) does not alter the quadratic scaling with N_t . The scaling with the number of basis functions changes from N_{bound}^p to $\max[N_{\text{bound}}^p, N_{\text{bound}}^q N_{\text{cont}}]$ where N_{cont} is the number of continuum states and $2 \leq q \leq 4$. Therefore, the proposed equations can be used to simulate a large class of molecules of current interest.

Assessment of NEGF approach: To demonstrate the reliability of the coupled NEGF Eqs. (4) we consider a 1D atom with soft Coulomb interactions. On the grid points $x_n = na$ with $|n| < N_{\text{grid}}/2$, the single-particle Hamiltonian reads $h(x_n, x_m) = \delta_{n,m}[2\kappa + V_n(x_n)] - \delta_{|n-m|,1}\kappa$, where the nuclear potential $V_n(x) = U_{\text{en}}/\sqrt{x^2 + a^2}$ for $|x| \leq R$ and $V_n(x) = 0$ otherwise. Electrons interact only in a box of length $2R$ centered around zero through $v(x, x') = ZU_{\text{ee}}/\sqrt{(x - x')^2 + a^2}$. The coupling to an external laser pulse is accounted for by adding $\delta_{nm}x_n E(t)$ to $h(x_n, x_m)$.

We take $N_{\text{grid}} = 400$ and (henceforth all quantities are expressed in atomic units) $a = 0.5$, $\kappa = 2$, $Z = 4$, $U_{\text{en}} = 2$, $U_{\text{ee}} = U_{\text{en}}/2$ and $R = 10a$. With four electrons the HF spectrum has $N_{\text{sys}} = 5$ bound states (per spin) and $N_{\text{cont}} = N_{\text{grid}} - N_{\text{sys}}$ continuum states. The occupied levels have energy $\epsilon_c = -4.33$ (core) and $\epsilon_v = -1.65$ (valence). The HF states are used to construct the Hamiltonian in Eqs. (1) and (2). The results obtained by solving the coupled NEGF Eqs. (4) [where ρ is a $N_{\text{sys}} \times N_{\text{sys}}$ matrix and f is a N_{cont} -dimensional vector] are benchmarked against NEGF calculations on the *full* grid (NEGF@grid). NEGF@grid simulations are performed by solving the original equation [26] $\dot{\rho} = -i[h_{\text{HF}}[\rho], \rho] - \mathcal{I}[\rho] - \mathcal{I}^\dagger[\rho]$ where all quantities are $N_{\text{grid}} \times N_{\text{grid}}$ matrices in the x_n -basis and \mathcal{I} is given by Eq. (A20) with $\Sigma = \Sigma_c$, see Appendix B for details. By construction, NEGF@grid simulations include the off-diagonal elements $h_{i\mu}$, $h_{\mu\mu'}$, $\mathbf{d}_{\mu\mu'}$ and all Coulomb integrals with two or more indices in the continuum. Notice that NEGF@grid scales cubically with N_{cont} and it is therefore not exportable to large systems.

In Fig. 2 we show the time-dependent (TD) occupation (per spin) of the core, n_c , and valence, n_v , levels. In the top panel we suddenly remove 4% of charge from the core, hence $\rho_{cc} \rightarrow \rho_{cc} - 0.04$, and let the system evolve *without* external fields. In the bottom panel the equilibrium system is driven by the external pulse

$$E(t) = E_0 \sin^2\left(\frac{\pi t}{T}\right) \sin(\Omega t) \quad (8)$$

with central frequency $\Omega = 6.2$, active from $t = 0$ until $t = T = 20$. The frequency is large enough for the energy of the photoelectron not to overlap with the energy of the Auger electron. The intensity has been chosen to have the same amount of expelled charge as in the case of the sudden removal: $E_0 = 2.0$ for NEGF@grid and $E_0 = 1.5$ for the coupled NEGF Eqs. (4) – the difference in the value of E_0 is due to the neglect of the

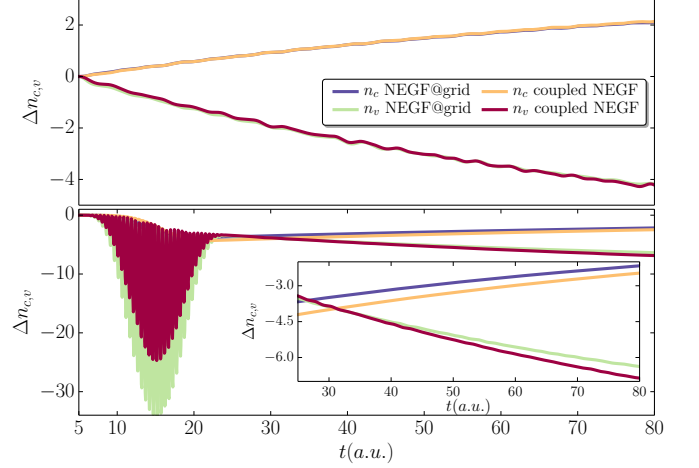


FIG. 2: Variation of the TD occupations (per spin) $n_c(t)$ [core, increasing blue (dark gray) and orange (light gray) curves] and $n_v(t)$ [valence, decreasing green (light gray) and red (dark gray) curves] calculated using NEGF@grid and coupled NEGF Eqs. (4) for the sudden creation of a core hole (top) and the action of a laser pulse (bottom). The inset shows a magnification of $n_c(t)$ and $n_v(t)$ after the end of the pulse. Vertical axes have been scaled up by a factor 10^2 .

dipole elements $d_{\mu\mu'}$ in Eq. (2). The results perfectly agree in the top panel whereas only a minor discrepancy is observed in the bottom panel. In both type of simulations the Auger decay slightly depends on how the core hole is created. In fact, the laser pulse is also responsible for expelling charge from the valence level, thereby hindering the refilling of the core. The core-hole lifetime agrees well with the inverse linewidth function $\Gamma(\epsilon_{\text{Auger}}) = 2\pi \sum_{\mu} |v_{c\mu vv}|^2 \delta(\epsilon_{\text{Auger}} - \epsilon_{\mu}) \simeq 10^{-2}$ in all cases. It is worth emphasizing that no time-local approximation of Σ_{Auger} would yield the behavior $n_c(t) = 1 - n_h e^{-\Gamma t}$. We performed TD HF simulations both in the grid basis and by solving Eqs. (4) with $\mathcal{J}_{\mu} = \Sigma_c = \Sigma_{\text{Auger}} = 0$, and found that $n_c(t)$ remains essentially constant (not shown). This is consistent with similar findings obtained in TDDFT using adiabatic xc potentials [19].

After the sudden creation of a core-hole the electronic density populates the continuum states φ_{μ} . In Fig. 3 we show the corresponding time-dependent occupations $f_{\mu}(t)$ versus their energy ϵ_{μ} . Again simulations have been performed using NEGF@grid (top panel) and the coupled NEGF Eqs. (4) (bottom panel). As time passes the total expelled charge increases and $f_{\mu}(t)$ gets peaked at the Auger energy $\epsilon_{\text{Auger}} = 2\epsilon_v - \epsilon_c \simeq 1$. The final profile of the peak has a width $\Gamma \equiv \Gamma(\epsilon_{\text{Auger}})$, independently of how the core hole is created (suddenly or due to a laser pulse). On the contrary, the photoelectron peak attains a width $\sim 2\pi/T$ immediately after the end of the pulse. We also observe that the exact energy of the Auger electron $\epsilon_{\text{Auger}}^{\text{exact}} = 2\epsilon_v - \epsilon_c - v_{vvvv}$ is not within reach the second-order approximation in Eq. (A13): the shift v_{vvvv}

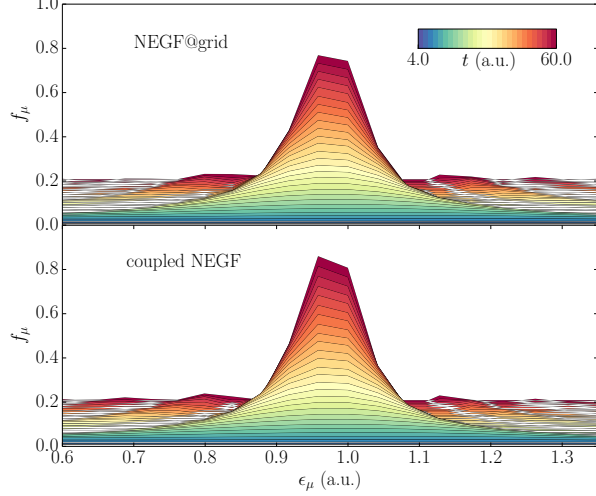


FIG. 3: Time-dependent occupations $f_\mu(t)$ of the continuum states versus their energy ϵ_μ after the sudden creation of a core hole. The results are obtained from the solution of the NEGF@grid equation (top) and coupled NEGF Eqs. (4) (bottom). In both cases the maximum occurs at $\epsilon_\mu = \epsilon_{\text{Auger}}$. Vertical axes have been scaled up by a factor 10^2 .

(due to the valence–valence repulsion) would require a T -matrix treatment [32, 33]. However, such shift has only a minor impact on the internal dynamics of 3D systems like, e.g., organic molecules, since the repulsion between two valence holes is typically less than 1 eV.

Auger wavepacket reconstruction: We now use the coupled NEGF Eqs. (4) to study the 1D atom on larger boxes (hence one- and two-electron integrals are calculated from HF states that spread over a large number of grid points). The output has been postprocessed to reconstruct the density of the Auger wavepacket according to $n_{\text{Auger}}(x, t) = \sum_{\mu\nu} \varphi_\mu^*(x) f_{\mu\nu}(t) \varphi_\nu(x)$, where $f_{\mu\nu}(t) = \langle \hat{c}_{\nu\sigma}^\dagger(t) \hat{c}_{\mu\sigma}(t) \rangle$ is the off-diagonal density matrix in the continuum sector. The latter is obtained by integrating the NEGF equation of motion (see SM for the derivation)

$$\dot{f}_{\mu\nu} = -i(\epsilon_\mu - \epsilon_\nu) f_{\mu\nu} - \mathcal{J}_{\mu\nu}[\rho, f] - \mathcal{J}_{\nu\mu}^*[\rho, f], \quad (9)$$

where $\mathcal{J}_{\mu\nu}$ is given by the right hand side of Eq. (6) after the replacement $K_{\mu\mu}^{\leq}(t, \bar{t}) f_\mu^{\geq}(\bar{t}) \rightarrow K_{\mu\nu}^{\leq}(t, \bar{t}) f_\nu^{\geq}(\bar{t})$.

In Fig. 4 we display the Auger wavepacket for $N_{\text{grid}} = 1600$ grid-points. In the top panel the core hole is suddenly created whereas in the middle panel the atom is driven by the ionizing laser of Eq. (8). The first observation is that the wavefront depends on the perturbation (sudden creation or laser), being steeper the shorter it takes to create the hole. The wavepacket moves rightward at the expected speed $v = \partial\epsilon/\partial p \simeq 2\sqrt{\kappa\epsilon_{\text{Auger}}} = 2.2$ and its length is approximately v/Γ far away from the nucleus. Interestingly, the tail of the wavepacket exhibits spatial ripples that tend to accumulate nearby the

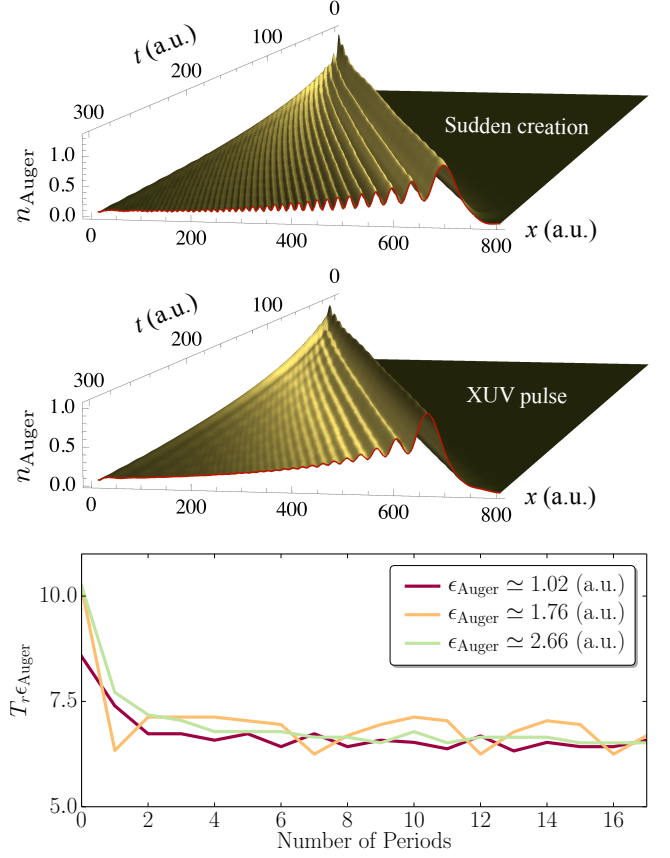


FIG. 4: Snapshots of the density of the Auger wavepacket after the sudden creation of a core hole (top) and the action of a laser pulse (middle). The bottom panel shows the period of the ripples at an interface versus the number of periods for three different values of range and strengths of the Coulomb force (see main text) yielding Auger energies $\epsilon_{\text{Auger}} = 1.02$ (red – dark gray), 1.76 (yellow – gray) and 2.66 (green – light gray).

origin. The amplitude of the ripples depends on the perturbation (sudden creation or laser) whereas their spacing is an *intrinsic* feature. In the bottom panel of Fig. 4 we show the period T_r of the ripples, i.e., the elapsing time between two consecutive maxima of $n_{\text{Auger}}(x_0, t)$, at the interface $x_0 = 30a$, versus the number of periods. We present results for three different values of range and strengths of the Coulomb force $(R, U_{\text{en}}, U_{\text{ee}}) = (10a, 2, 1), (100a, 2.6, 2.08), (10a, 2.7, 2.025)$ yielding Auger energies $\epsilon_{\text{Auger}} = 1.02, 1.76, 2.66$ respectively. In all cases we find that T_r attains a finite limit given by

$$T_r = 2\pi/\epsilon_{\text{Auger}}. \quad (10)$$

The occurrence of ripples and the intrinsic period T_r is not an artifact of the self-energy approximation. These features as well as the overall shape of the Auger wavepacket are indeed confirmed by CI calculations. Starting at time $t = 0$ with the photoexcited state $|\Phi_x\rangle = \hat{c}_{c\uparrow}^\dagger \hat{c}_{v\downarrow}^\dagger \hat{c}_{v\uparrow}^\dagger |0\rangle$ and evolving with the Hamiltonian

in Eq. (1) one finds $n_{\text{Auger}}(x, t) = |\varphi_{\text{Auger}}(x, t)|^2$ with $\varphi_{\text{Auger}}(x, t) = \sum_{\mu} a_{\mu}(t) \varphi_{\mu}(x)$ and

$$a_{\mu}(t) \simeq -v_{c\mu\nu\nu} e^{-iE_{\mu}t} \frac{e^{i(\epsilon_{\mu} - \epsilon_{\text{Auger}} + i\Gamma/2)t} - 1}{\epsilon_{\mu} - \epsilon_{\text{Auger}} + i\Gamma/2}. \quad (11)$$

The CI Auger wavepacket is in excellent agreement with NEGF, see Appendix C. In the Appendix C we further show that the ripples occur even in two or three dimensions and, therefore, they are a fingerprint of the Auger electron.

To summarize, we have included Auger decays in a first-principles NEGF approach to simulate the UCM dynamics of molecules driven by attosecond pulses. The computational effort is comparable to that of previous NEGF implementations [26–28], thereby allowing for studying systems with tens of active electrons up to tens of femtoseconds. Benchmarks in 1D atoms demonstrate that both qualitative and quantitative aspects are well captured. We also predict a highly asymmetric profile of the Auger wavepacket with a spatial extension of the order v/Γ and superimposed ripples with temporal period $T_r = 2\pi/\epsilon_{\text{Auger}}$.

Although the fundamental equations have been derived for finite systems, the proposed NEGF approach can be extended to deal with periodic systems too. In this context the equation of motion for the single particle density matrix opens the possibility to develop current-density functional theories that include dissipation and thermalization.

Acknowledgements G.S. and E.P. acknowledge EC funding through the RISE Co-ExAN (Grant No. GA644076). E.P. also acknowledges funding from the European Union project MaX Materials design at the eXascale H2020-EINFRA-2015-1, Grant Agreement No. 676598 and Nanoscience Foundries and Fine Analysis-Europe H2020-INFRAIA-2014-2015, Grant Agreement No. 654360. F.C. and A.R. acknowledge financial support from the European Research Council (ERC-2015-AdG-694097), Grupos Consolidados (IT578-13) and European Union Horizon 2020 program under Grant Agreement 676580 (NOMAD).

Appendix A: Derivation of NEGF equations in HF basis

The starting point is the equation of motion for the Green's function $\mathcal{G}(z, z')$ with times z, z' on the Keldysh contour. For the Hamiltonian in Eqs. (1) and (2) it is convenient to write \mathcal{G} and the correlation self-energy Σ in a block form

$$\mathcal{G}(z, z') = \begin{pmatrix} G(z, z') & \Delta(z, z') \\ \bar{\Delta}(z, z') & C(z, z') \end{pmatrix}, \quad (A1)$$

$$\Sigma(z, z') = \begin{pmatrix} \Sigma_G(z, z') & \Sigma_{\Delta}(z, z') \\ \bar{\Sigma}_{\Delta}(z, z') & \Sigma_C(z, z') \end{pmatrix}, \quad (A2)$$

where G is a matrix with indices in the bound sector, C is a matrix with indices in the continuum sector and $\Delta, \bar{\Delta}$ are the off-diagonal blocks. The blocks of the self-energy have the same structure. For the self-energy we make the following approximation

(i) All self-energy diagrams containing Δ or $\bar{\Delta}$ propagators are set to zero (see below for the justification).

From the approximation (i) it follows that $\Sigma_{\Delta} = \bar{\Sigma}_{\Delta} = 0$ and that the Hartree-Fock (HF) potential has indices only in the bound sector since the Coulomb integrals in \hat{H}^{eq} have at most one index in the continuum. The explicit form of the HF potential is

$$V_{\text{HF},ij}(z) = -i \sum_{mn} G_{nm}(z, z^+) w_{imnj}, \quad (A3)$$

where $w_{imnj} \equiv 2v_{imnj} - v_{ijnm}$.

The equations of motion for the different blocks of \mathcal{G} then read (in matrix form)

$$\begin{aligned} \left[i \frac{d}{dz} - h_{\text{HF}}(z) \right] G(z, z') - (\mathbf{E}(z) \cdot \mathbf{d}) \bar{\Delta}(z, z') \\ = \delta(z, z') + \int d\bar{z} \Sigma_G(z, \bar{z}) G(\bar{z}, z') \end{aligned} \quad (A4)$$

$$\begin{aligned} \left[i \frac{d}{dz} - \mathcal{E} \right] \bar{\Delta}(z, z') - (\mathbf{E}(z) \cdot \mathbf{d}) G(z, z') \\ = \delta(z, z') + \int d\bar{z} \Sigma_C(z, \bar{z}) \bar{\Delta}(\bar{z}, z') \end{aligned} \quad (A5)$$

$$\left[i \frac{d}{dz} - \mathcal{E} \right] C(z, z') = \delta(z, z') + \int d\bar{z} \Sigma_C(z, \bar{z}) C(\bar{z}, z') \quad (A6)$$

where in Eq. (A4) we have defined the nonequilibrium single-particle HF Hamiltonian

$$h_{\text{HF}} = h + V_{\text{HF}} + \mathbf{E} \cdot \mathbf{d}, \quad (A7)$$

and in the last two equations we have defined the matrix $\mathcal{E}_{\mu\nu} = \delta_{\mu\nu} \epsilon_{\mu}$. The blocks of the dipole matrix are unambiguously determined by the contractions and we do therefore use the same symbol for all four blocks. Notice that no coupling with the electric field appears in Eq. (A6) since we set $\mathbf{d}_{\mu\mu'} = 0$ in Eq. (2).

Next we observe that if the energy-window of the photoelectron does not overlap with that of the Auger electron then we can make the approximation:

$$(ii) \Sigma_C(z, \bar{z}) \bar{\Delta}(\bar{z}, z') \simeq 0.$$

With the approximation (ii) we easily integrate Eq. (A5) and obtain

$$\bar{\Delta}_{\mu j}(z, z') = \sum_n \int d\bar{z} C_{\mu}^0(z, \bar{z}) (\mathbf{E}(\bar{z}) \cdot \mathbf{d}_{\mu n}) G_{nj}(\bar{z}, z'), \quad (A8)$$

where C^0 is the solution of Eq. (A6) with $\Sigma_C = 0$. Since \mathcal{E} is diagonal so is C^0 .

Inserting Eq. (A8) into Eq. (A4) we get

$$\left[i \frac{d}{dz} - h_{\text{HF}}(z) \right] G(z, z') = \delta(z, z') + \int d\bar{z} [\Sigma_G(z, \bar{z}) + \Sigma_{\text{ion}}(z, \bar{z})] G(\bar{z}, z'), \quad (\text{A9})$$

where we have defined the ionization self-energy

$$\Sigma_{\text{ion},ij}(z, \bar{z}) \equiv \sum_{\mu} (\mathbf{E}(z) \cdot \mathbf{d}_{i\mu}) C_{\mu}^0(z, \bar{z}) (\mathbf{E}(\bar{z}) \cdot \mathbf{d}_{\mu j}). \quad (\text{A10})$$

The diagrammatic representation of the ionization self-energy is displayed in the bottom diagram of Fig. 1(b) where, to avoid a proliferation of different symbols, we used G_{μ}^0 instead of C_{μ}^0 (in the main text we also used $G_{\mu\nu}$ instead of $C_{\mu\nu}$). Notice that Σ_{ion} vanishes for times at which the external pulse is zero.

We now have to specify the approximation for the correlation self-energy. For weakly interacting closed systems (no continuum states) the self-consistent second-Born approximation (2B) has been shown to be accurate in several nonequilibrium situations [27, 34–42]. The very same approximation describes Auger scatterings provided that we also consider interaction lines with one index in the continuum [30, 31]. We therefore approximate Σ_G and Σ_C as the sum of the 2B diagrams. It is easy to show that for a \mathcal{G} initially block diagonal (no electrons in the continuum in the ground state) the off-diagonal blocks remain zero for all times in the 2B approximation. This justifies the approximation (i).

The 2B diagrams for Σ_G can be split into diagrams with interaction lines having all indices in the bound sector (v) and diagrams with interaction lines having one index in the continuum sector (v^A):

$$\Sigma_G = \Sigma_c + \Sigma_{\text{Auger}}. \quad (\text{A11})$$

Using the Feynman rules, see top and middle panel of Fig. 5, one finds

$$\Sigma_{c,ij}(z, z') = \sum_{mn,pq,sr} v_{irpm} w_{nqsj} \times G_{mn}(z, z') G_{pq}(z, z') G_{sr}(z', z), \quad (\text{A12})$$

and

$$\begin{aligned} \Sigma_{\text{Auger},ij}(z, z') &= \sum_{mn,pq} \sum_{\mu} G_{mn}(z, z') \\ &\times [C_{\mu\nu}(z, z') G_{pq}(z', z) (v_{iqm\mu}^A w_{\nu npj}^A + v_{iq\mu m}^A w_{\nu npj}^A) \\ &+ G_{pq}(z, z') C_{\mu\nu}(z', z) v_{i\nu pm}^A w_{nq\mu j}^A] \end{aligned} \quad (\text{A13})$$

The correlation self-energy Σ_c is also given in the top diagram of Fig. 1(b).

The 2B diagrams for Σ_C do instead contain only v^A interaction lines since both indices of Σ_C are in the continuum sector. From the bottom diagram of Fig. 5 one

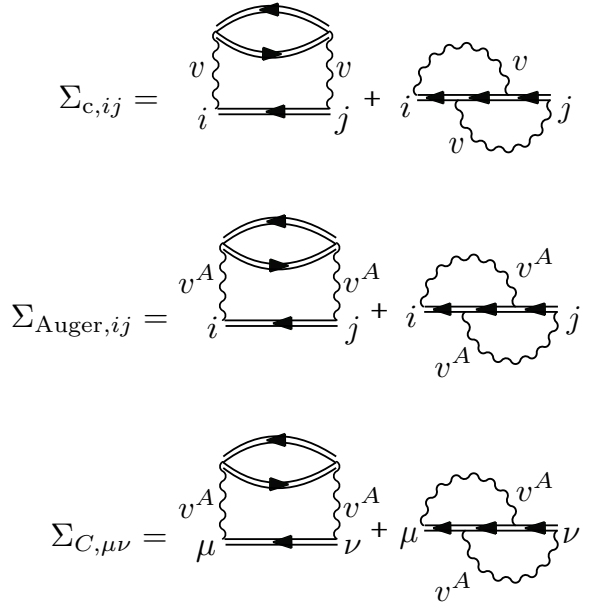


FIG. 5: Self-energy diagrams with indices in the bound sector for intramolecular scattering (top) and Auger scattering (middle). Self-energy diagrams for Auger electrons (bottom).

finds

$$\begin{aligned} \Sigma_{C,\mu\nu}(z, z') &= \sum_{mn,pq,sr} v_{\mu r p m}^A w_{n q s \nu}^A \\ &\times G_{mn}(z, z') G_{pq}(z, z') G_{sr}(z', z) \end{aligned} \quad (\text{A14})$$

For a short and weak laser pulse the off-diagonal matrix elements of C are small. We therefore make the approximation

$$(iii) \ C_{\mu\nu} \simeq \delta_{\mu\nu} C_{\mu} \text{ in } \Sigma_{\text{Auger}}$$

Implementing (iii) in Eq. (A13) and extracting the lesser/greater component we get precisely the self-energy in Eq. (5).

To summarize, with the approximations (i-iii) the equations of motion become

$$\left[i \frac{d}{dz} - h_{\text{HF}}(z) \right] G(z, z') = \delta(z, z') + \int d\bar{z} \Sigma(z, \bar{z}) G(\bar{z}, z') \quad (\text{A15})$$

$$\left[i \frac{d}{dz} - \mathcal{E} \right] C(z, z') = \delta(z, z') + \int d\bar{z} \Sigma_C(z, \bar{z}) C(\bar{z}, z') \quad (\text{A16})$$

where in Eq. (A15) we have defined

$$\Sigma \equiv \Sigma_c + \Sigma_{\text{ion}} + \Sigma_{\text{Auger}}. \quad (\text{A17})$$

Taking the adjoint of Eqs. (A15,A16), summing the resulting equations to Eqs. (A15,A16) and evaluating the

result in $z = z^+ = t$ we get the equation of motion for the density matrices $\rho_{ij}(t) = -iG_{ij}(z, z^+)$ and $f_{\mu\nu}(t) = -iC_{\mu\nu}(z, z^+)$:

$$\dot{\rho} = -i[h_{\text{HF}}, \rho] - \mathcal{I} - \mathcal{I}^\dagger, \quad (\text{A18})$$

$$\dot{f}_{\mu\nu} = -i(\epsilon_\mu - \epsilon_\nu)f_{\mu\nu} - \mathcal{J}_{\mu\nu} - \mathcal{J}_{\nu\mu}^*, \quad (\text{A19})$$

where

$$\mathcal{I}(t) = \int_0^t d\bar{t} [\Sigma^>(t, \bar{t})G^<(\bar{t}, t) - \Sigma^<(t, \bar{t})G^>(\bar{t}, t)], \quad (\text{A20})$$

$$\mathcal{J}(t) = \int_0^t d\bar{t} [\Sigma_C^>(t, \bar{t})C^<(\bar{t}, t) - \Sigma_C^<(t, \bar{t})C^>(\bar{t}, t)]. \quad (\text{A21})$$

Equations (A18,A19) do not close on ρ and f since the right hand side depends on G and C calculated at different times. To close the equations we make the Generalized Kadanoff-Baym Ansatz [29] (GKBA). According to the GKBA we can replace all G^{\lessgtr} and C^{\lessgtr} appearing in \mathcal{I} and \mathcal{J} with

$$G^{\lessgtr}(t, \bar{t}) = \mp [G^{\text{R}}(t, t')\rho^{\lessgtr}(t') - \rho^{\lessgtr}(t)G^{\text{A}}(t, t')], \quad (\text{A22})$$

$$C^{\lessgtr}(t, \bar{t}) = \mp [C^{\text{R}}(t, t')f^{\lessgtr}(t') - f^{\lessgtr}(t)C^{\text{A}}(t, t')], \quad (\text{A23})$$

where $\rho^< = \rho$, $\rho^> = 1 - \rho$ and similarly $f^< = f$, $f^> = 1 - f$. For the retarded/advanced Green's function we consider the HF approximation according to which

$$G^{\text{R}}(t, t') = [G^{\text{A}}(t', t)]^\dagger = -i\theta(t - t')\mathcal{T} \left[e^{-i \int_{t'}^t d\bar{t} h_{\text{HF}}(\bar{t})} \right], \quad (\text{A24})$$

$$C_{\mu\nu}^{\text{R}}(t, t') = [C_{\nu\mu}^{\text{A}}(t', t)]^* = -i\delta_{\mu\nu}\theta(t - t')e^{-i\epsilon_\mu(t - t')}. \quad (\text{A25})$$

Since h_{HF} is a functional of ρ we see that Eqs. (A18,A19) become nonlinear integro-differential equations for $\rho_{ij}(t)$ and $f_{\mu\nu}(t)$. Notice also that in the equation for ρ the dependence on f is only through the diagonal elements $f_\mu \equiv f_{\mu\mu}$ appearing in Σ_{Auger} , due to the approximation (iii). If we set $\mu = \nu$ in Eq. (A19) then for the right hand side to depend only on f_μ we have to make the approximation

$$(iv) \ f_{\mu\nu} = \delta_{\mu\nu}f_\mu \text{ in } \mathcal{J}$$

which is consistent with the approximation (iii).

It is easy to show that in this way the equation for ρ becomes the first of Eqs. (4) and that the equation for $f_{\mu\nu}$ becomes Eq. (9), which for $\mu = \nu$ reduces to the second of Eqs. (4).

Appendix B: NEGF@grid versus coupled NEGF calculations

To assess the accuracy of the approximations made at the level of the Hamiltonian with Eqs. (1,2) and at the level of NEGF with (i-iv), we considered a 1D atom on a grid. In the grid basis the total Hamiltonian in second quantization reads

$$\begin{aligned} \hat{H}(t) = & \sum_{mn} \psi_\sigma^\dagger(x_m) h(x_m, x_n) \psi_\sigma(x_n) \\ & + \frac{1}{2} \sum_{mn} \psi_\sigma^\dagger(x_m) \psi_{\sigma'}^\dagger(x_n) v(x_m, x_n) \psi_{\sigma'}(x_n) \psi_\sigma(x_m) \\ & + E(t) \sum_{\sigma} x_m \psi_\sigma^\dagger(x_m) \psi_\sigma(x_m). \end{aligned} \quad (\text{B1})$$

where the one-particle Hamiltonian $h(x, x')$ and the interaction $v(x, x')$ are defined in the main text. The equation of motion for the density matrix in grid basis $\rho(x_m, x_n, t) = G(x_m, z; x_n, z^+)$ in the 2B approximation is

$$\begin{aligned} \dot{\rho}(x_m, x_n, t) = & -i \sum_p [h_{\text{HF}}(x_m, x_p, t)\rho(x_p, x_n, t) \\ & - \rho(x_m, x_p, t)h_{\text{HF}}(x_p, x_n, t)] \\ & - \mathcal{I}_g(x_m, x_n, t) - \mathcal{I}_g^*(x_n, x_m, t). \end{aligned} \quad (\text{B2})$$

In Eq. (B2) we have the HF Hamiltonian in grid basis

$$h_{\text{HF}}(x_m, x_p, t) = h(x_m, x_p) + V_{\text{HF}}(x_m, x_p, t) + \delta_{mp}E(t)x_m, \quad (\text{B3})$$

with HF potential

$$\begin{aligned} V_{\text{HF}}(x_m, x_p, t) = & 2\delta_{nm} \sum_q v(x_m, x_q)\rho(x_q, x_q, t) \\ & - v(x_m, x_p)\rho(x_m, x_p, t), \end{aligned} \quad (\text{B4})$$

and the collision integral in grid basis

$$\begin{aligned} \mathcal{I}_g(x_m, x_n, t) = & \sum_p \int_0^t d\bar{t} [\Sigma_g^>(x_m, t; x_p, \bar{t})G^<(x_p, \bar{t}; x_n, t) \\ & - \Sigma_g^<(x_m, t; x_p, \bar{t})G^>(x_p, \bar{t}; x_n, t)], \end{aligned} \quad (\text{B5})$$

with the 2B self-energy

$$\begin{aligned} \Sigma_g^{\lessgtr}(x_m, t; x_p, \bar{t}) = & \sum_{rs} v(x_m, x_r)v(x_p, x_s) \\ & \times \left[2G^{\lessgtr}(x_m, t; x_p, \bar{t})G^{\lessgtr}(x_r, t; x_s, \bar{t})G^{\gtrless}(x_s, \bar{t}; x_r, t) \right. \\ & \left. - G^{\lessgtr}(x_m, t; x_s, \bar{t})G^{\gtrless}(x_s, \bar{t}; x_r, t)G^{\lessgtr}(x_r, t; x_p, \bar{t}) \right]. \end{aligned} \quad (\text{B6})$$

The NEGF@grid results have been obtained by solving Eq. (B2) with lesser/greater Green's function evaluated at the GKBA level. Except that for the 2B approximation to Σ_g , no other approximation has been made. For

a system with N_{grid} points this require to propagate and store matrices $N_{\text{grid}} \times N_{\text{grid}}$.

In order to apply the coupled NEGF scheme based on Eqs. (4) we first solve the self-consistent HF problem and extract the equilibrium bound eigenfunctions $\varphi_i(x_n)$ and continuum eigenfunctions $\varphi_\mu(x_n)$ of energy ϵ_i and ϵ_μ respectively. The HF eigenfunctions are then used to calculate the matrix elements in the bound sector of the one-particle Hamiltonian

$$h_{ij} = \sum_{mn} \varphi_i^*(x_m) h(x_m, x_n) \varphi_j(x_n), \quad (\text{B7})$$

the dipole operator

$$d_{ij} = \sum_m \varphi_i^*(x_m) x_m \varphi_j(x_m), \quad (\text{B8})$$

and the Coulomb repulsion

$$v_{ijpq} = \sum_{mn} \varphi_i^*(x_m) \varphi_j^*(x_n) v(x_m, x_n) \varphi_p(x_n) \varphi_q(x_m). \quad (\text{B9})$$

The continuum HF eigenfunctions are used to calculate the bound-continuum matrix elements of the dipole operator

$$d_{i\mu} = \sum_m \varphi_i^*(x_m) x_m \varphi_\mu(x_m), \quad (\text{B10})$$

and the Coulomb repulsion responsible for Auger scatterings

$$v_{ijp\mu}^A = \sum_{mn} \varphi_i^*(x_m) \varphi_j^*(x_n) v(x_m, x_n) \varphi_p(x_n) \varphi_\mu(x_m). \quad (\text{B11})$$

With this information we approximate the original Hamiltonian in Eq. (B1) in accordance with Eqs. (1,2), i.e.,

$$\begin{aligned} \hat{H}(t) = & \sum_{ij} h_{ij} \hat{c}_{i\sigma}^\dagger \hat{c}_{j\sigma} + \frac{1}{2} \sum_{ijpq} v_{ijpq} \hat{c}_{i\sigma}^\dagger \hat{c}_{j\sigma'}^\dagger \hat{c}_{p\sigma'} \hat{c}_{q\sigma} \\ & + \sum_{\mu\sigma} \epsilon_\mu \hat{c}_{\mu\sigma}^\dagger \hat{c}_{\mu\sigma} + \sum_{ijp\mu} v_{ijp\mu}^A \left(\hat{c}_{i\sigma}^\dagger \hat{c}_{j\sigma'}^\dagger \hat{c}_{p\sigma'} \hat{c}_{\mu\sigma} + \text{h.c.} \right) \\ & + E(t) \sum_{ij} d_{ij} \hat{c}_{i\sigma}^\dagger \hat{c}_{j\sigma} + E(t) \sum_{i\mu} \left(d_{i\mu} \hat{c}_{i\sigma}^\dagger \hat{c}_{\mu\sigma} + \text{h.c.} \right) \end{aligned} \quad (\text{B12})$$

where $\hat{c}_{i\sigma}$ ($\hat{c}_{\mu\sigma}$) are annihilation operators for an electron in the HF orbital φ_i (φ_μ) with spin σ . Of course, had we included in Eq. (B12) the off-diagonal one-electron terms containing $h_{i\mu}$, $h_{\mu\mu'}$ and $d_{\mu\mu'}$ and the interaction terms containing $v_{ij\mu\mu'}$, $v_{i\nu\mu\mu'}$ and $v_{\nu'\nu\mu\mu'}$ we would have got the same Hamiltonian as in Eq. (B1) but in the HF basis.

With the approximate Hamiltonian in Eq. (B12) we solve the coupled NEGF equations (4) which, we emphasize again, have been derived by making the additional approximations (i-iv) of the previous section. The

agreement between the full-grid simulations and the simulations based on Eqs. (4) indicate that the latter are enough to capture qualitatively and quantitatively the physics of the Auger decay.

We observe that in the grid simulations the self-energy Σ_g contains all possible scatterings, including those contained in the self-energies Σ_c and Σ_{Auger} of the coupled NEGF scheme. Furthermore, in the grid simulations no ionization self-energy appears since the photoionization is accounted for by explicitly including all grid points (even those far away from the nucleus). In other words, *all* elements $\rho(x_m, x_n, t)$ are coupled and propagated in time.

Appendix C: CI versus coupled NEGF calculations

To further check the quality of the NEGF Eqs. (4) we have also solved the time-dependent problem using a Configuration Interaction (CI) expansion.

The neutral 1D atom described in the main text of the paper has four electrons, two in the core and two in the valence levels. We are interested in suddenly removing a core electron of, say, spin down, and in studying how the system evolves with the Hamiltonian in Eq. (B12). For the CI expansion we use the following three-body states

$$|\Phi_x\rangle = \hat{c}_{c\uparrow}^\dagger \hat{c}_{v\downarrow}^\dagger \hat{c}_{v\uparrow}^\dagger |0\rangle, \quad (\text{C1})$$

$$|\Phi_g\rangle = \hat{c}_{c\uparrow}^\dagger \hat{c}_{c\downarrow}^\dagger \hat{c}_{v\uparrow}^\dagger |0\rangle, \quad (\text{C2})$$

$$|\Phi_\mu\rangle = \hat{c}_{c\uparrow}^\dagger \hat{c}_{c\downarrow}^\dagger \hat{c}_{\mu\uparrow}^\dagger |0\rangle, \quad (\text{C3})$$

describing the initially photoionized state (Φ_x), the cationic ground state (Φ_g) and the Auger states (Φ_μ). We expand the state of the system at time t according to

$$|\Psi(t)\rangle = a_x(t)|\Phi_x\rangle + a_g(t)|\Phi_g\rangle + \sum_{\mu} a_{\mu}(t)|\Phi_{\mu}\rangle, \quad (\text{C4})$$

and impose the initial condition $a_x(0) = 1$ and $a_{\mu}(0) = 0$. Using the fact that in the HF basis h_{HF} is diagonal, it is easy to show that the cationic ground state decouples and the dynamics is governed by the equations below

$$i\dot{a}_x = E_x a_x + \sum_{\mu} v_{c\mu v v} a_{\mu}, \quad (\text{C5})$$

$$i\dot{a}_{\mu} = v_{c\mu v v} a_x + E_{\mu} a_{\mu}. \quad (\text{C6})$$

The three-body energies are

$$E_x = 2\epsilon_v + \epsilon_c - v_{cccc} - 4v_{cvvc} + 2v_{cvcv} - v_{vvvv}, \quad (\text{C7})$$

$$E_{\mu} = \epsilon_{\mu} + 2\epsilon_c - v_{cccc} - 4v_{cvvc} + 2v_{cvcv}, \quad (\text{C8})$$

where the HF energies of the core and valence levels are given by

$$\epsilon_c = h_{cc} + v_{cccc} + 2v_{cvvc} - v_{cvcv}, \quad (\text{C9})$$

$$\epsilon_v = h_{vv} + v_{vvvv} + 2v_{vccv} - v_{vccv}. \quad (\text{C10})$$

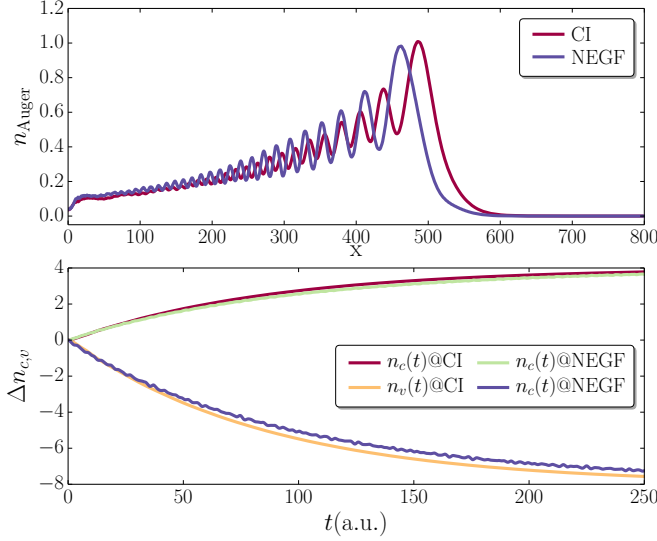


FIG. 6: Auger wavepacket (top) and variation of the occupations of the core and valence levels (bottom) in CI and in coupled NEGF. Same parameters as in top panel of Fig. 4.

The energy $\epsilon_{\text{Auger}} = \epsilon_{\mu_A}$ of the Auger electron is determined by the condition $E_{\mu_A} = E_x$ which yields

$$\epsilon_{\text{Auger}} = 2\epsilon_v - \epsilon_c - v_{vvvv} \quad (\text{C11})$$

as it should. The red-shift v_{vvvv} is due to the repulsion of the two holes in the final state. In order to capture this red-shift using Many-Body Perturbation Theory (MBPT) one should go beyond the 2B approximation for the self-energy and consider the T -matrix approximation in the particle-particle sector [32, 33]. We observe, however, that for weakly correlated molecules, like organic molecules and biomolecules, the magnitude of the valence-valence repulsion is typically less than 1 eV; hence, neglecting this repulsion does not substantially affect the dynamics during the first ten of femtoseconds or so.

For the 1D atom the valence-valence repulsion is mainly responsible for reducing the speed of the Auger electron. The form of the Auger wavepacket as well as the time-dependent behavior of the refilling of the core-hole are not altered if we set $v_{vvvv} = 0$ in Eq. (C7). For a fair comparison with the coupled NEGF Eqs. (4) we therefore solve Eqs. (C5,C6) using $E_x^{2B} = E_x + v_{vvvv}$ in place of E_x . In Fig. 6 we compare the Auger wavepacket (top panel) and the occupation of the core and valence levels (bottom panels) calculated using CI and the coupled NEGF equations (4). Also in this case the agreement is rather satisfactory.

The analytic calculation can be carried on further if we assume that the broadening

$$\Gamma(\omega) = 2\pi \sum_{\mu} |v_{c\mu vv}|^2 \delta(\omega - \epsilon_{\mu}) \quad (\text{C12})$$

is a weakly dependent function of ω for $\omega \simeq \epsilon_{\text{Auger}}$. In this case it is straightforward to show that the amplitudes

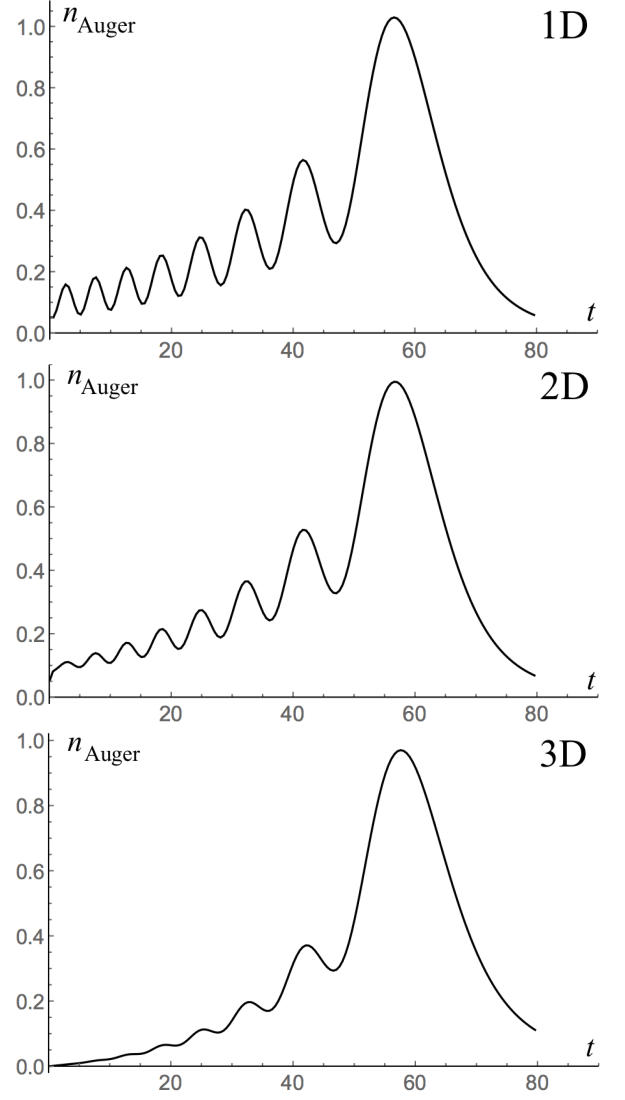


FIG. 7: Auger wavepacket (in arbitrary units) for $\Gamma = 0.05$ and $\epsilon_{\text{Auger}} = 1$ after a time $t = 50$ from the sudden removal of a core electron. Top: $n_{\text{Auger}}(r, t)$ in 1D. Middle: $rn_{\text{Auger}}(r, t)$ in 2D. Bottom: $r^2 n_{\text{Auger}}(r, t)$ in 3D.

a_{μ} are given by

$$a_{\mu}(t) = -v_{c\mu vv} e^{-iE_{\mu}t} \frac{e^{i(\epsilon_{\mu} - \epsilon_{\text{Auger}} + i\Gamma/2)t} - 1}{\epsilon_{\mu} - \epsilon_{\text{Auger}} + i\Gamma/2} \quad (\text{C13})$$

which coincides with Eq. (11). The occurrence of ripples on the tail of the Auger wavepacket stems from the structure of the a_{μ} 's. In fact, the ripples are independent of the dimension of the system and of the details of the continuum states in the vicinity of the nucleus. As an example, let $\mu = \mathbf{p}$ be the momentum in D dimension and let us use planewaves $\varphi_{\mu}(\mathbf{r}) = \varphi_{\mathbf{p}}(\mathbf{r}) = e^{i\mathbf{p} \cdot \mathbf{r}}$ for the continuum states. We further consider a free dispersion $\epsilon_{\mu} = \epsilon_{\mathbf{p}} = p^2/2$ and, for simplicity, an Auger interaction $v_{c\mu vv} = v_{c\mathbf{p}vv}$ independent of \mathbf{p} so that $a_{\mu} = a_p$ depends only on the modulus $p = |\mathbf{p}|$ of the momentum,

see Eq. (C13). Then, the Auger wavepacket is spherically symmetric and its density is given by

$$n_{\text{Auger}}(r, t) = \left| \int \frac{d^D p}{(2\pi)^D} a_p(t) e^{i\mathbf{p} \cdot \mathbf{r}} \right|^2. \quad (\text{C14})$$

In Fig. 7 we show $n_{\text{Auger}}(r, t)$ for $\Gamma = 0.05$ and an

Auger energy $\epsilon_{\text{Auger}} = 1$ after a time $t = 50$ from the sudden removal of the core electron. The figure shows $n_{\text{Auger}}(r, t)$ in 1D (top), $rn_{\text{Auger}}(r, t)$ in 2D (middle) and $r^2 n_{\text{Auger}}(r, t)$ in 3D (bottom). In all cases we appreciate the occurrence of ripples although they tend to get smeared out as the dimension increases.

-
- [1] F. Calegari, D. Ayuso, A. Trabatttoni, L. Belshaw, S. De Camillis, S. Anumula, F. Frassetto, L. Polletto, A. Palacios, P. Decleva, et al., *Science* **346**, 336 (2014), ISSN 0036-8075, URL <http://science.sciencemag.org/content/346/6207/336>.
 - [2] M. Uiberacker, T. Uphues, M. Schultze, A. J. Verhoeef, V. Yakovlev, M. F. Kling, J. Rauschenberger, N. M. Kabachnik, H. Schröder, M. Lezius, et al., *Nature* **446**, 627 (2007).
 - [3] A. I. Kuleff and L. S. Cederbaum, *Journal of Physics B: Atomic, Molecular and Optical Physics* **47**, 124002 (2014), URL <http://stacks.iop.org/0953-4075/47/i=12/a=124002>.
 - [4] A. I. Kuleff, N. V. Kryzhevoi, M. Pernpointner, and L. S. Cederbaum, *Phys. Rev. Lett.* **117**, 093002 (2016), URL <https://link.aps.org/doi/10.1103/PhysRevLett.117.093002>.
 - [5] J. Breidbach and L. S. Cederbaum, *The Journal of Chemical Physics* **118**, 3983 (2003), <http://dx.doi.org/10.1063/1.1540618>, URL <http://dx.doi.org/10.1063/1.1540618>.
 - [6] N. V. Golubev and A. I. Kuleff, *Phys. Rev. A* **91**, 051401 (2015), URL <https://link.aps.org/doi/10.1103/PhysRevA.91.051401>.
 - [7] K. Nagaya, H. Iwayama, A. Sugishima, Y. Ohmasa, and M. Yao, *Applied Physics Letters* **96**, 233101 (2010), <https://doi.org/10.1063/1.3442483>, URL <https://doi.org/10.1063/1.3442483>.
 - [8] M. Kutzner, V. Maycock, J. Thorarinson, E. Panitz, and J. A. Robertson, *Phys. Rev. A* **66**, 042715 (2002), URL <https://link.aps.org/doi/10.1103/PhysRevA.66.042715>.
 - [9] T. Uphues, M. Schultze, M. F. Kling, M. Uiberacker, S. Hendel, U. Heinzmann, N. M. Kabachnik, and M. Drescher, *New Journal of Physics* **10**, 025009 (2008), URL <http://stacks.iop.org/1367-2630/10/i=2/a=025009>.
 - [10] M. Drescher, M. Hentschel, R. Kienberger, M. Uiberacker, V. Yakovlev, A. Scrinzi, T. Westerwalbesloh, U. Kleineberg, U. Heinzmann, and F. Krausz, *Nature* **419**, 803 (2002), article, URL <http://dx.doi.org/10.1038/nature01143>.
 - [11] S. Zharebtsov, A. Wirth, T. Uphues, I. Znakovskaya, O. Herrwerth, J. Gagnon, M. Korbman, V. S. Yakovlev, M. Vrakking, M. Drescher, et al., *Journal of Physics B: Atomic, Molecular and Optical Physics* **44**, 105601 (2011).
 - [12] J. M. Schins, P. Breger, P. Agostini, R. C. Constantinescu, H. G. Muller, G. Grillon, A. Antonetti, and A. Mysyrowicz, *Phys. Rev. Lett.* **73**, 2180 (1994), URL <https://link.aps.org/doi/10.1103/PhysRevLett.73.2180>.
 - [13] O. Smirnova, V. S. Yakovlev, and A. Scrinzi, *Phys. Rev. Lett.* **91**, 253001 (2003), URL <https://link.aps.org/doi/10.1103/PhysRevLett.91.253001>.
 - [14] A. K. Kazansky, I. P. Sazhina, and N. M. Kabachnik, *Journal of Physics B: Atomic, Molecular and Optical Physics* **42**, 245601 (2009), URL <http://stacks.iop.org/0953-4075/42/i=24/a=245601>.
 - [15] A. K. Kazansky, I. P. Sazhina, and N. M. Kabachnik, *Journal of Physics B: Atomic, Molecular and Optical Physics* **44**, 215601 (2011), URL <http://stacks.iop.org/0953-4075/44/i=21/a=215601>.
 - [16] E. Runge and E. K. U. Gross, *Phys. Rev. Lett.* **52**, 997 (1984), URL <https://link.aps.org/doi/10.1103/PhysRevLett.52.997>.
 - [17] C. Ullrich, *Time-Dependent Density-Functional Theory* (Oxford University Press, Oxford, 2012).
 - [18] N. T. Maitra, *The Journal of Chemical Physics* **144**, 220901 (2016), <https://doi.org/10.1063/1.4953039>, URL <https://doi.org/10.1063/1.4953039>.
 - [19] C. S. Cucinotta, D. Hughes, and P. Ballone, *Phys. Rev. B* **86**, 045114 (2012), URL <https://link.aps.org/doi/10.1103/PhysRevB.86.045114>.
 - [20] The inadequacy of the adiabatic approximation is easily understandable. The Auger electron adds to the main quasi-particle peak a secondary peak in the spectral function of the parent cation. An adiabatic approximation can, at most, renormalize the main quasi-particle peak.
 - [21] L. P. Kadanoff and G. A. Baym, *Quantum statistical mechanics: Green's function methods in equilibrium and nonequilibrium problems* (Benjamin, 1962).
 - [22] G. Stefanucci and R. van Leeuwen, *Nonequilibrium Many-Body Theory of Quantum Systems: A Modern Introduction* (Cambridge University Press, Cambridge, 2013).
 - [23] P. Myöhänen, A. Stan, G. Stefanucci, and R. van Leeuwen, *Phys. Rev. B* **80**, 115107 (2009), URL <https://link.aps.org/doi/10.1103/PhysRevB.80.115107>.
 - [24] P. Myöhänen, A. Stan, G. Stefanucci, and R. van Leeuwen, *EPL (Europhysics Letters)* **84**, 67001 (2008), URL <http://stacks.iop.org/0295-5075/84/i=6/a=67001>.
 - [25] S. Latini, E. Perfetto, A.-M. Uimonen, R. van Leeuwen, and G. Stefanucci, *Phys. Rev. B* **89**, 075306 (2014).
 - [26] E. Perfetto, A.-M. Uimonen, R. van Leeuwen, and G. Stefanucci, *Phys. Rev. A* **92**, 033419 (2015), URL <https://link.aps.org/doi/10.1103/PhysRevA.92.033419>.
 - [27] E. V. Boström, A. Mikkelsen, C. Verdozzi, E. Perfetto, and G. Stefanucci, *Nano Lett.* **18**, 785 (2018), <https://doi.org/10.1021/acs.nanolett.7b03995>, URL <https://doi.org/10.1021/acs.nanolett.7b03995>.
 - [28] E. Perfetto, D. Sangalli, A. Marini, and G. Stefanucci, *The Journal of Physical Chemistry Letters* **9**, 1353

- (2018), <https://doi.org/10.1021/acs.jpcllett.8b00025>, URL <https://doi.org/10.1021/acs.jpcllett.8b00025>.
- [29] P. Lipavský, V. Špička, and B. Velický, Phys. Rev. B **34**, 6933 (1986), URL <https://link.aps.org/doi/10.1103/PhysRevB.34.6933>.
- [30] C.-O. Almbladh, A. L. Morales, and G. Grossmann, Phys. Rev. B **39**, 3489 (1989), URL <https://link.aps.org/doi/10.1103/PhysRevB.39.3489>.
- [31] C.-O. Almbladh and A. L. Morales, Phys. Rev. B **39**, 3503 (1989), URL <https://link.aps.org/doi/10.1103/PhysRevB.39.3503>.
- [32] M. Cini, Solid state communications **88**, 1101 (1993).
- [33] G. A. Sawatzky, Phys. Rev. Lett. **39**, 504 (1977), URL <https://link.aps.org/doi/10.1103/PhysRevLett.39.504>.
- [34] K. Balzer, S. Bauch, and M. Bonitz, Phys. Rev. A **82**, 033427 (2010), URL <https://link.aps.org/doi/10.1103/PhysRevA.82.033427>.
- [35] K. Balzer, S. Hermanns, and M. Bonitz, EPL (Europhysics Letters) **98**, 67002 (2012), URL <http://stacks.iop.org/0295-5075/98/i=6/a=67002>.
- [36] N. Säkkinen, M. Manninen, and R. van Leeuwen, New Journal of Physics **14**, 013032 (2012), URL <http://stacks.iop.org/1367-2630/14/i=1/a=013032>.
- [37] S. Hermanns, N. Schlünzen, and M. Bonitz, Phys. Rev. B **90**, 125111 (2014), URL <https://link.aps.org/doi/10.1103/PhysRevB.90.125111>.
- [38] N. Schlünzen and M. Bonitz, Contrib. Plasma Phys. **56**, 5 (2016), ISSN 1521-3986, URL <http://dx.doi.org/10.1002/ctpp.201610003>.
- [39] M. Hopjan, D. Karlsson, S. Ydman, C. Verdozzi, and C.-O. Almbladh, Phys. Rev. Lett. **116**, 236402 (2016), URL <https://link.aps.org/doi/10.1103/PhysRevLett.116.236402>.
- [40] Y. B. Lev and D. R. Reichman, EPL (Europhysics Letters) **113**, 46001 (2016), URL <http://stacks.iop.org/0295-5075/113/i=4/a=46001>.
- [41] N. Schlünzen, J.-P. Joost, F. Heidrich-Meisner, and M. Bonitz, Phys. Rev. B **95**, 165139 (2017), URL <https://link.aps.org/doi/10.1103/PhysRevB.95.165139>.
- [42] A.-M. Uimonen, E. Khosravi, A. Stan, G. Stefanucci, S. Kurth, R. van Leeuwen, and E.K.U. Gross, Phys. Rev. B **84**, 115103 (2011).